Electrochemical Immunosensor Based on the Interactions Between Polypyrrole and Cobalt (II) Salicylaldiimine Dendrimer

Lindsay Wilson[*], Juanita vam Wyk[1] Candice Rassie, Natasha Ross, Christopher Sunday, Hlamulo R. Makelane, Mawethu Bilibana, Tesfaye Waryo, Selwyn Mapolie[2], Priscilla G. Baker, Emmanuel I. Iwuoha

Department of Chemistry, University of the Western Cape, Bellville, 7535, Cape Town, South Africa
[1]Currently at Department of Chemistry, University of the Witwatersrand, Johannesburg, South Africa.
[2]Currently at Department of chemistry, Stellenbosch University, Stellenbosch, South Africa.
[*]E-mail: 2724554@myuwc.ac.za

Transglutaminase is primarily involved with activation and progression of coeliac disease through the ingestion of gluten which initiates the production of antibodies against transglutaminase. This results in the damage of the small intestine reducing the diffusion of digested foods into the blood vessels. The diagnosis of coeliac disease can be done by the measurement of antibodies against transglutaminase. This work involves the development of an electrochemical immunosensor for the detection of anti-transglutaminase antibodies. A platinum modified polypyrrole-cobalt (II) salicyladiimine metallodendrimer composite capped with transglutaminase and bovine serum albumin was used for the determination of anti-transglutaminase antibodies. Surface roughness of 879.24 nm, 76.55 nm and 364.27 nm for polypyrrole, cobalt (II) salicyladiimine metallodendrimer and their respective composite in conjunction with cyclic voltammetry showed that such composites provide a suitable micro-environment for monitoring antibody-antigen interactions. Electrochemical impedance spectroscopy parameters such as exchange current and heterogeneous rate constant are used to evaluate immunosensor where the rate constants were 2.7×10^{-6} cm^2 s^{-1}, 4.6×10^{-6} cm^2 s^{-1} and 4.16×10^{-6} cm^2 s^{-1} for cobalt (II) salicyladiimine metallodendrimer, polypyrrole and their composite. Impedimetric immunosensor gave a limit of detection of 201 ng mL^{-1} and linear range of 10^{-5} - 10^{-4} mg mL^{-1} with correlation coefficient of 0.948.

1. INTRODUCTION

The identification of transglutaminase (tTG) as an auto antigen of celiac disease (CD), lead to the extensive study on the pathogenesis and diagnosis of CD. The ingestion of gluten from wheat or barley is deamidated by tTG, in genetically predisposed persons. This results in the damage of the small intestine through loss of absorptive villi and hyperplasia [1-2]. The predisposition of human leukocyte antigen (HLA) molecules DQ2 and DQ8 are major genetic factors influencing the progression of CD with the presence of tTG [3-4]. Transglutaminase, a calcium dependent enzyme, is involved in the catalysis of protein crosslinkages and other various physiological functions, namely glutamine to a protein containing a lysine residue through glutamine donor and glutamine acceptors. Such that tTG displays high specificity to such glutamine substrates [5]. The use of tTG for diagnosis of CD derives from the enzyme complex with gliadin which triggers an immune response against tTG and gliadin. The immune response triggers the expression of serum antibodies against tTG and gliadin [6]. The fundamental diagnostic tool for CD is performing a small intestine biopsy or serological tests that are tedious and expensive. The development of highly sensitive and specific assays that use autoantibodies against tTG is the pivotal step in future screening for CD. Electrochemical immunosensors offer highly sensitive and selective biosensing of protein biomarkers in early diagnosis and progression tests [7].

Dendrimers offer new chemical and physical properties of different nature to linear polymers. Dendrimers may also be used as bridging ligands between transition metal complexes, where metal ions are bonded to two different molecules at the periphery, as metallo-dendrimers. Voltammetry enables the study of surface-confined electroactive dendrimers (metallo-dendrimers) films [8-9]. Hence the type of metal incorporated, specific location within the dendrimer (periphery or at core) influences structure, shape, size and electroactivity. Cobalt (II) Shiff base complexes were found to be suitable platform for biomolecules on a metallic electrode surface [10]. The interaction of such complexes with biomolecules can be studied through voltammetry and mainly impedance spectroscopy. To further improve the electrochemical platform, Schiff base complexes can form stable composites with conducting polymers [11-12]. These new materials exhibit high stability and they maintain their structural integrity.

This work represents a simple and direct immunosensor development method for the detection of anti-tTG antibodies. It involves the electropolymerization of pyrrole and cobalto-salicyldiimine in situ, forming a nanocomposite of high stability and suitability for biomolecule immobilization. Polypyrrole and Co(II) complexes have good biocompatibility and their respective nanocomposite hybrid material improves there efficiency as electron catalysts for monitoring bio-recognition events [13-15]. The antigen (tTG) is drop casted onto Pt/PPY-Co(II) and left to adhere to the platform through physisorption. Electrochemical impedance spectroscopy is used to monitor the interaction between the nanocomposite and tTG. The antigen-antibody complex formation is well monitored with EIS. The changes in the charge transfer resistance, double layer capacitance as well change in phase angle is used to screen the antigen-antibody interaction immunosensor performance.

2. EXPERIMENTAL

2.1. Reagents

Pyrrole was purchased from Sigma-Aldrich and purified through double distillation. Transglutaminase (tTG) antigen from guine pig liver, Anti-Transglutaminase Type II antibody produced in goat, Sodium dihydrogen orthophosphate, Disodium hydrogen orthophosphate, Ethanol (99.8%) and Lithium perchlorate (LiClO$_4$) were purchased from Sigma Aldrich. Acetone (99.0%) was purchased from Kimix. Bovine Serum Albumin was purchased from Fluka. All solutions used for experiments were prepared with Millipore (Milli-Q purification). Cobalt (II) salicyladiimine metallodendrimer (Co(II)SDD) was synthesized by Juanita vam Wyk (16) and was stored at room temperature before use. Phosphate buffer (pH 7.0) was produced from 0.1 M Sodium dihydrogen orthophosphate (NaH$_2$PO$_4$) and 0.1 M Disodium hydrogen orthophosphate (Na$_2$HPO$_4$), with the pH adjusted by mixing of adequate volumes of each solution. Lithium perchlorate solutions were prepared to 0.1 M solutions in Millipore water. A second buffer (Phosphate Tween buffer, pH 7.0.) consisting of 10 mM phosphate, 137 mM NaCl and 0.05% (V/V) Tween 20.

2.2. Apparatus and electrochemical setup

The electrochemical polymerization and nanocomposite (immunosensor platform) preparations were done with cyclic voltammetry. All electrochemical characterization, Cyclic Voltammetry and Square Wave Voltammetry was done with a BAS 100/W electrochemical analyser from Bioanalyser systems Inc. A three electrode system was used consisting of a platinum working electrode (Pt), platinum wire as counter electrode and Ag/AgCl (3 M NaCl) as reference electrode. Before electrochemical measurements were performed, solutions were purged with argon gas and blanketed with argon atmosphere. Fourier transform infrared spectrums were acquired using a FTIR-Spectrometer Perkin Elmer (Spectrum 100). A Nicolet Evolution 100 UV-visible spectrometer was used for all UV-vis absorption measurements of samples in quartz cuvettes and polymers on transparent indium tin oxide electrodes. Atomic Force Microscopy images were done with NanoSurf easyScan 2 system.

2.3. Preparation of conductive supports

2.3.1. Preparation of polypyrrole modified platinum electrode

Electropolymerization of 0.1 M pyrrole in 0.1 M LiClO$_4$ was done using Cyclic Voltammetry within a potential range of -400 to 700 mV for 20 cycles. During the polymerization, greater positive potentials were avoided since over-oxidation of polypyrrole (PPy) would occur which decreases the conductivity of the polymer. The increase in current waves depicts the growth of polypyrrole films on the surface of the electrode. The polymer film adhered strongly to the electrode surface. As electro-oxidation occurs, conjugated bonds increases the stability of the polymer film since electron transfer

and positive charge injection with doping and undoping of anions into the film increases the ease of generating a conductive film.

2.3.2. Preparation of polypyrrole cobalto-salicyladiimine nanocomposite support.

The nanocomposite was prepared by electropolymerization of 0.1 M pyrrole solution and 5 mM cobalto-salicyldiimine complex in 0.1 M $LiClO_4$ was done for preparation of nanocomposite between -400 to 700 mV for 20 cycles. In situ electropolymerisation was enhanced by the SDD-Co (II) complex acting as an electrochemical catalyst. Electron transfer between polymer and complex results in shift in peak potentials. This is due to the Co(II) being oxidized to Co(III) and being reduced back to Co(II).

2.3.3. Preparation of Immunosensor

After the preparation of the nano-composite platform, 40 µL of transglutaminase solution (0.2 mg mL^{-1} prepared in 0.1 M phosphate buffer) was immobilized onto the platform and incubated for 1 h at 25 °C. The tTG antigen solution was then removed by rinsing with phosphate-tween 20 buffer. The nanocomposite with recognition layer was characterized with cyclic voltammetry and impedance spectroscopy. The detection commenced by performing a blocking step, where BSA was incubated for 1 h on the modified electrode followed by incubation of anti-tTG antibody for 1 h. Electrochemical impedance spectroscopy was used for the detection of anti-tTG antibodies.

3. RESULTS AND DISCUSSION

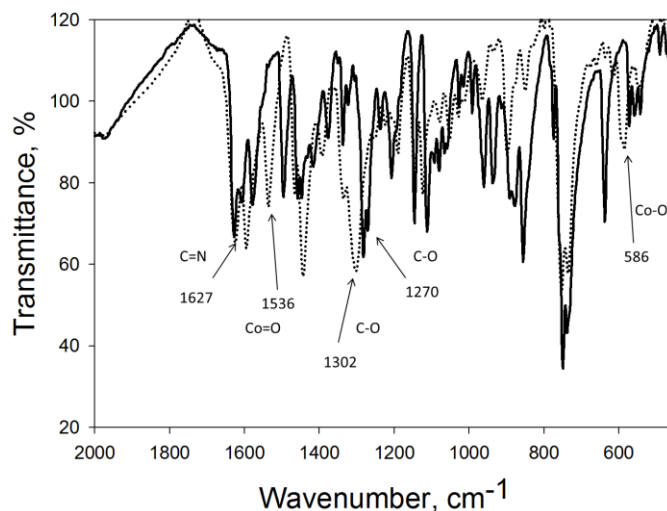*3.1. Spectroscopic characterization of immunosensor layers.*

Figure 1. FT-IR spectrum of SDD (solid line) and Co(II)-SDD (dotted-line).

A shift in the C=N stretching band at 1627 cm^{-1} in SDD to 1624 cm^{-1} in cobalt Schiff base complex was seen, as well as an appearance of new band at 1536 cm^{-1} in the spectrum of Co(II), which suggests coordination of N-Co. Coordination is further confirmed by the shift in the C–O stretching vibration of the phenoxy group from the region 1269 - 1279 cm^{-1} to a higher frequency range which indicates M–O coordination. A new band at 586 cm^{-1} in the Co(II) spectrum suggesting Co-O stretching. These shifts from SDD ligand to the incorporation of cobalt shows that cobalt is bound and incorporated into the SDD ligand.

The UV–vis spectra in Fig.2 shows the values of the wavelength of maximum absorbance are 371 nm and 409 nm for SDD and SDD–Co(II), respectively. The absorption at 371 nm is related to π - π * intra-SDD transition and that at 409 nm is related to d–π * charge transfer transition in the SDD–Co(II) metal complex. There are no absorbance wavelengths that indicate further d-d* transitions indicating that the Co is in its +2 state.
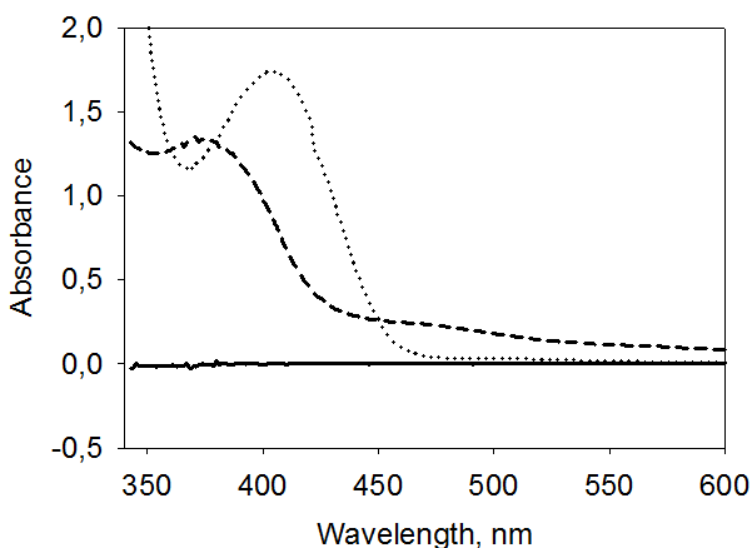

Figure 2. UV-vis absorbance of solvent (solid line), SDD (dotted line), Co(II)-SDD (sliced line) in 1:1 (v/v) acetone-ethanol solution.

3.2. Morphology studies

Atomic force microscopy was done to determine surface morphology of polypyrrole, cobalt (II) metallodendrimer and their nanocomposite. The nature of surface morphologies of polypyrrole are influenced by type of dopants used such as p-toluensulfonate, dodecylsulfate anions and nitrates. This work involved using perchlorate anions as dopant. Fig.3 b shows the topographical image for PPy modified platinum electrode. Clusters of polymer film are observed in comparison to bare Pt with perchlorate anion used as dopant. Regular voids and wells are observed since perchlorate anions are more readily incorporated into polymer film through the electropolymerisation process. The surface roughness was calculated from the line plot with Nanosurf easyscan 2 AFM software and is seen in table 1 below.

Table 1. Calculated surface roughness from AFM.

Surface Roughness		
	Ra	Rq
Bare Pt electrode	20.46 nm	28.55 nm
Pt/PPy	879.24 nm	996.67 nm
Pt/Co(II)SDD	76.755 nm	99. 17 nm
Pt/PPy-Co(II)SDD	364.27 nm	421.17 nm

Surface A is clearly the least rough for bare Pt electrode. The electropolymerization of pyrrole onto Pt electrode increased the surface roughness to 879.24 nm. Surface area for Pt/Co(II)SDD and Pt/PPy-Co(II)SDD was 76.75 nm and 364.27 nm respectively. The reduction in surface area for the composite is due to the inclusion of Co(II)SDD within polypyrrole. These values co-inside with topographical images seen in Fig.3.
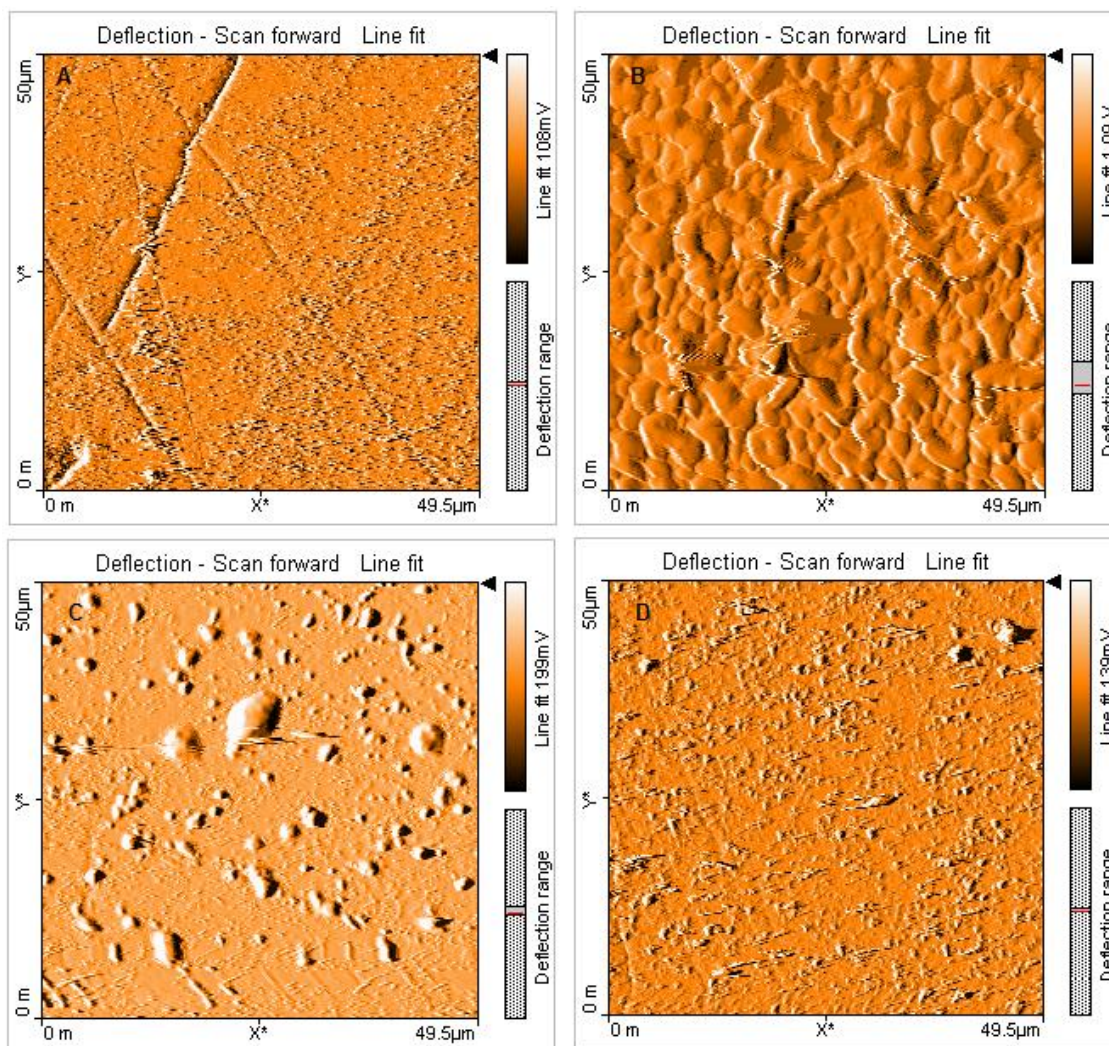

Figure 3. AFM topographical images of, a) bare Pt electrode, b) PPy modified platinum electrode, c) Co(II)SDD modified platinum electrode, d) PPy-Co(II)SDD modified platinum electrode.

3.3. Electrochemical characterization

3.3.1. Polypyrrole modified platinum electrode

After the electropolymerization process, a stable and thin polymer layer of polypyrrole is shown on platinum electrode. Different concentrations of pyrrole were used for the electropolymerization process, and it was found that 0.1 M of pyrrole gave the best response. Fig.4 shows the cyclic voltammogram for Pt/PPY in 0.1 M phosphate buffer in at different scan rates.
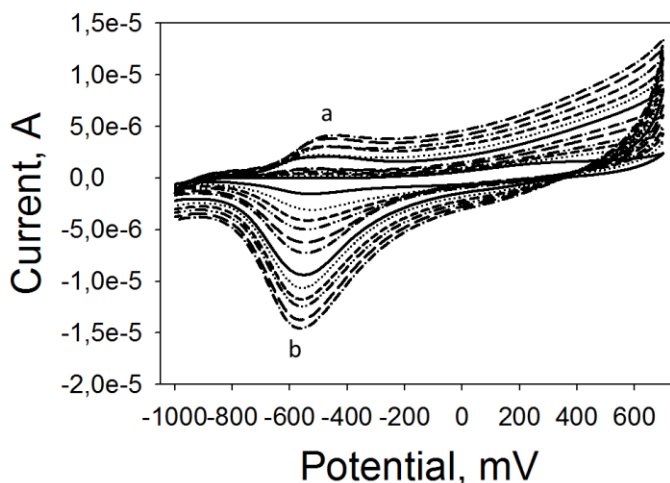

Figure 4. Cyclic voltammograms of polypyrrole modified platinum electrode in 0.1 M phosphate buffer at 10 to 200 mV s^{-1}.

A pair of quasi-reversible peaks are observed with a reduction wave from -280 mV to -680 mV and an oxidation wave at -200 mV to -570 mV. The reduction peak is more dominant since electron transfer between polymer and platinum electrode occurs more favourably on reduction in comparison to other electrodes . No hydrogen adsorption and desorption is observed in the respect regions. This is due to the electron transfer effect of the polymer which leaves positive holes. Reduction diffusion coefficients were calculated to be 6.3539×10^{-9} m^2 s^{-1} and oxidation diffusion coefficients to be 9.2156×10^{-10} m^2 s^{-1} which suggests fast mass transfer.

Cyclic voltammetry of the polypyrrole modified platinum electrode in 0.1 M LiClO$_4$ was done to further study the thin film material. Two oxidation peaks are observed at -540 mV (a) and 180 mV (a') in Fig. 5. As scan rate increases the oxidation peak at 180 mV (a') increases to higher oxidation potential of 400 mV. The predominance of peak a' derives from the formation of the bipolaron PPy^{++}. The pair of quasi-reversible redox peaks observed at -580 mV (b) and -540 mV (a) occurs from polypyrrole being oxidised from its neutral state PPy^0 to PPy$^+$ and on reduction from PPy$^+$ to PPy^0. Electron transfer was founded to be 2 at 100 mV s^{-1} and decreased to 1 electron transfer process at lower scan rates. A plot of log of current vs log of scan rates indicates that the thin polymer film is adsorbed onto the surface of the platinum electrode.
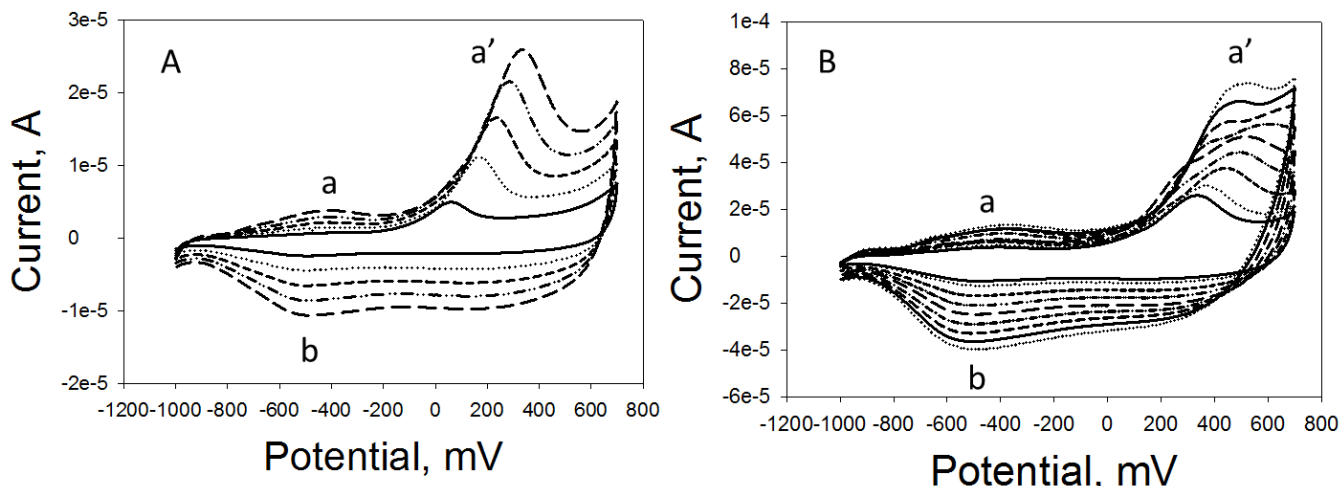
Figure 5. Scan rate study for cyclic voltammograms of polypyrrole modified platinum electrode in 0.1 M LiClO$_4$, A) 10 - 50 mV s^{-1}, B) 50 - 200 mV s^{-1}.

The acidity of LiClO$_4$ should be taken into account since it is more acidic than phosphate buffer solutions of pH 7. Two processes occur during oxidation/reduction of polypyrrole. Firstly, electron transfer to and from polypyrrole and secondly the diffusion of counterions in an out of polypyrrole. The proton exchange at high acidity occurs at a faster rate hence there is a dominance of an oxidation peak, namely peak a'.

3.3.2. Cobalt(II) salicyladiimine metallodendrimer modified platinum electrode

Cobalt (II) SDD showed relatively small alterations to peak potentials when compared to bare platinum electrode in 0.1 M phosphate buffer solution.
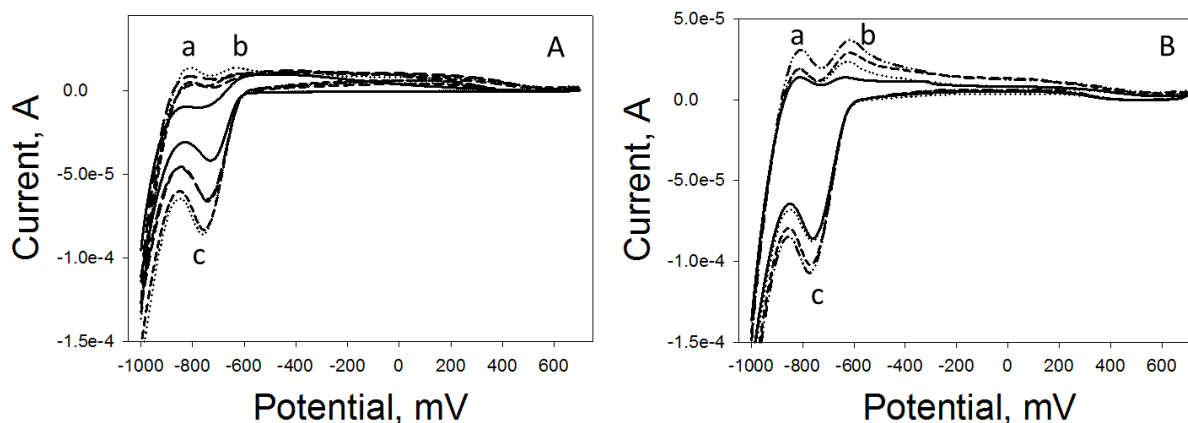

Figure 6. Cyclic voltammograms of Co(II)SDD modified platinum electrode in 0.1 M phosphate buffer, A) 10 - 50 mV s^{-1}, B) 50 - 100 mV s^{-1}.

The well known platinum peaks in Fig. 11 (A) at -742.3 mV, -620.3 mV and -824.3 mV are shifted to -773.3 mV, -606.7 mV and -832.7 mV in Fig. 6. A potential shift of 13.6 mV in the oxidation peak of Pt when modified with Co(II)SDD results from a one electron transfer for Co(II)/Co(III) process. A 36.6% decrease in anodic current is observed compared to bare Pt. The potential shift of the reduction peak to higher reduction potential by 30.3 mV shows a one electron transfer process for reducing Co(III) back to Co(II). It is well known that the +2 oxidation state of cobalt is more stable than the +3 state, therefore the reduction wave between Pt electrode and Co(II) complex has a 13 % drop in anodic peak current. These changes can be attributed to the redox systems of the Schiff base.

Taking into account that the hydrogen adsorption and desorption occurs at these potentials. As scan rate increases the peak potentials remains constant showing a surface bound material.

3.3.3. Nanocomposite modified platinum electrode

The in-situ electropolymerization of PPy and Co(II)SDD showed more stable and reproducible behaviour seen in Fig.8. Since cobalt Schiff base is entrapped in the polymer, the redox process of Co(II)/Co(III) became reversible at higher scan rates. The electroactive layer shows high stability since peak potentials are independent of scan rate. Quasi-reversible peaks are observed at -550 mV.
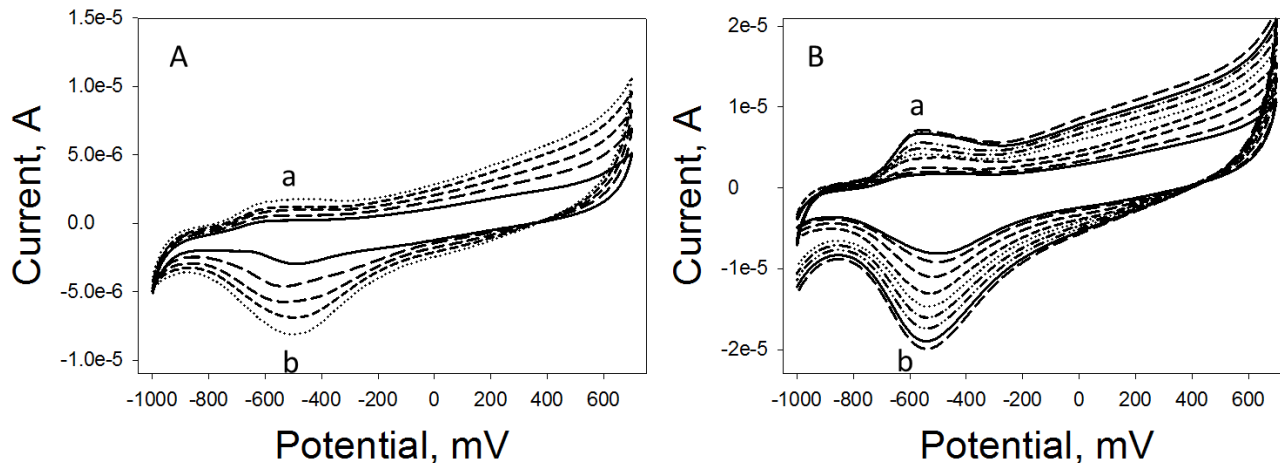

Figure 8. Cyclic voltammograms of nanocomposite (Pt/PPy-Co(II)SDD) modified platinum electrode in 0.1 M phosphate buffer, A) 10 - 50 mV s^{-1}, B) 50 - 200 mV s^{-1}.

The nanocomposite modified platinum electrode was characterized in a 0.1 M LiClO$_4$ solution. In Fig. 9, reversible redox peaks at –420 mV (c and d) are observed and a further oxidation peak at 180 mV (c'). For slow scan rates, the peak potential is dependent on scan rate for second oxidation peak. Surface confined polymer film is observed by peak potential c and d remaining constant. The presence

of cobalt complexed enhanced electron transfer in the polymeric chain, observed by increased in peak c and peak d linearly with increase in scan rate. At higher scan rates, the reduction peak at -420 mV enlargers into a wave-like broad peak. This is due to the inherent electron transfer between PPy-Co(II)SDD and electrolyte solution.
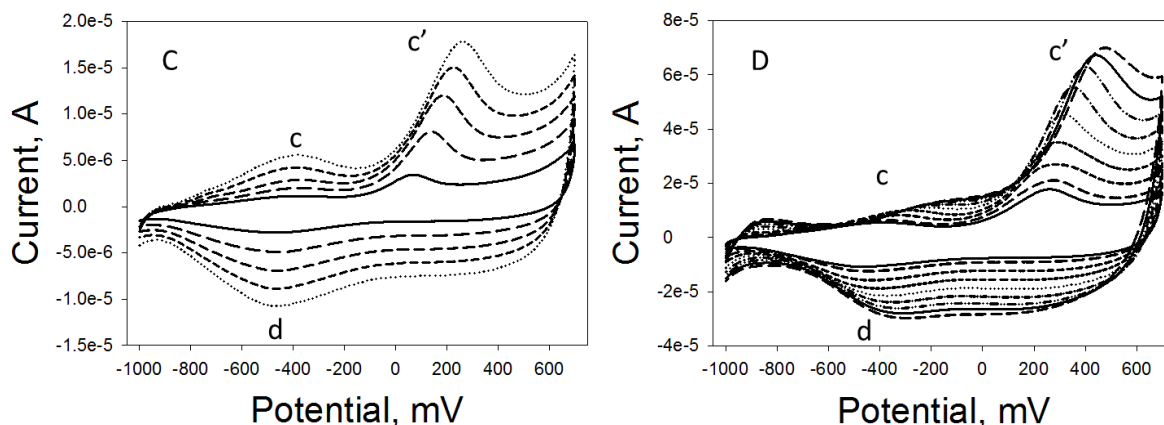

Figure 9. Cyclic voltammograms of nanocomposite (Pt/PPy-Co(II)SDD) modified platinum electrode in 0.1 M LiClO, C) 10 - 50 mV s^{-1}, D) 50 - 200 mV s^{-1}.

The electrochemical character of the nanocomposite shows good stability and a suitable platform for biomolecule immobilization. The oxidation of Co(II) to Co(III) increased oxidation efficiency of PPy to PPy $^{+}$ at slower scan rates. At fast scan rates, peak d broadens into a current wave between -400 mV and 400 mV compared to Pt/PPy (Fig.5B) with the current wave from -600 mV to 400 mV. The presence of Co(III) shifted reduction potential wave of PPy from -600 mV (Fig.5B) to -400 mV (Fig.9D). The less reductive potentials shows that Co(III) enhanced the electron transfer across the PPy polymeric chain.

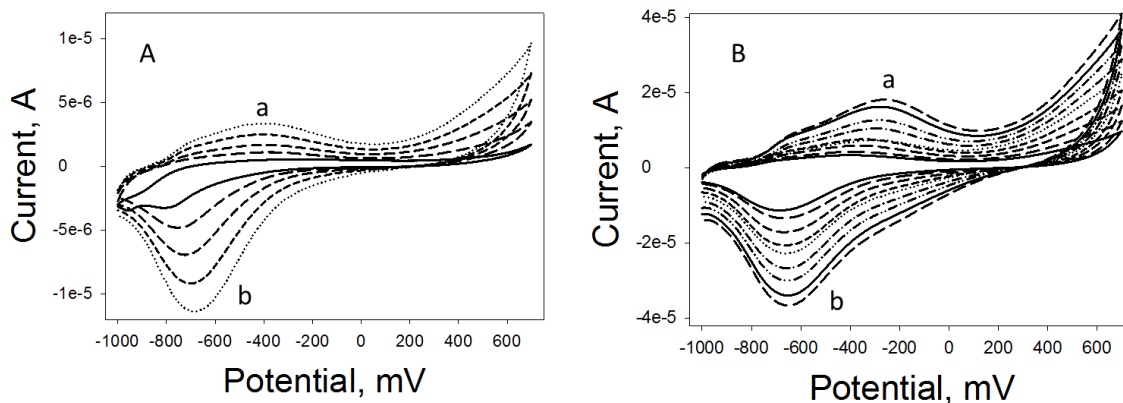### 3.3.4. Characterization of Pt/PPy-Co(II)SDD platform with tTG

Figure 10. Cyclic voltammograms of nanocomposite(Pt/PPy-Co(II)SDD) modified platinum electrode at, A) 10 - 50 mV s^{-1}, B) 50 - 200 mV s^{-1} in phosphate buffer.

The immobilization of transglutaminase on the surface of prepared electrode platform showed a decrease in oxidation peaks seen for Pt/PPy and Pt/PPy-Co(II)SDD.

The reduction process indicates good electron transfer between the immobilized tTG and electrode platform. Oxidation process showed an increase in tTG oxidation capability by peak potentials shifting to less negative potentials with increase in scan rate. Reduction at peak b in Fig. 10 corresponds to a 100 mV increase compared to Pt/PPy-Co(II)SDD, shows a two electron transfer process. Proteins are known to hinder electron transfer processes with secondary reactions occurring. This is seen in two oxidation peaks at higher scan rates with peak potentials of -600 mV and -400 mV. The oxidation peak at -400 mV is due to charge transfer between nanocomposite electrode and tTG.
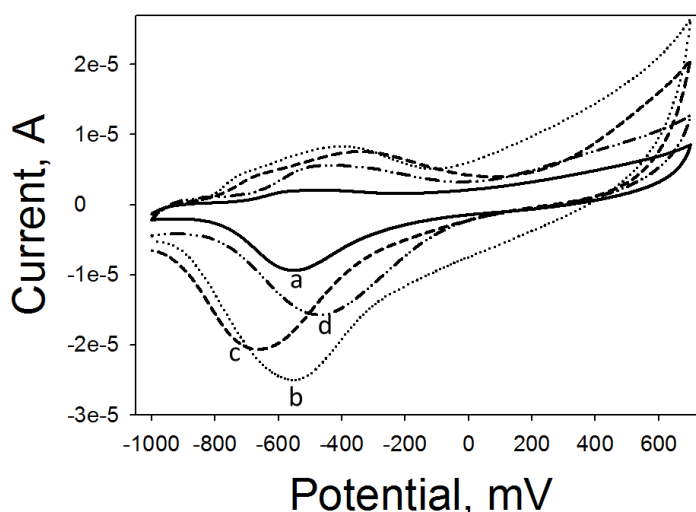
Figure 11. A) Comparison of Cyclic voltammograms of (a) Pt/PPy, (b) Pt/PPy-Co(II)SDD, (c) Pt/PPy-Co(II)SDD/tTG, (d) Pt/PPy-Co(II)SDD/tTG/BSA.

Fig.11 represents the different cyclic voltammograms for the step by step modification of the platinum electrode to the immunosensor containing transglutaminase. As observed, Pt/PPy-Co(II)SDD shows the highest cathodic current (b) compared to Pt/PPy and Pt/Co(II)SDD. As the protein, transglutaminase, is adsorbed on the surface of the electrode, the cathodic current decreased since electrons require further travelling distance and has higher steric hindrance. Cathodic peak potential difference between that of Pt/PPy to Pt/PPy-Co(II)SDD is 30 mV, and between Pt/PPy-Co(II)SDD and Pt/PPy-Co(II)SDD/tTG is 110 mV. The increase from nanocomposite to the immunosensor arises from secondary electron transfer reactions occurring at the electrode/electrolyte interface.

3.4. Electrochemical Impedance Spectroscopy

EIS is a powerful technique for electronic and analytical description of nanomaterials at the electrode/electrolyte interface. The charge dissipation provides information about interactions between electroactive materials and biological components, as well as biological interactions such as antibody-

antigen interactions. Electrodes modified with chemical biocompatible molecules can be monitored through their respective charge transfer resistance as well as capacitance behaviour. The resultant impedance spectra are assessed by fitting the data to an equivalent circuit model with imaginary components' that represent the physic-chemical process and bio-physic-chemical process as well [17]. A shortened Randles equivalent circuit is used to fit the impedance data for evaluation of the processes that occur. The circuit consists of solution resistance (Rs) models the solution resistance, charge transfer resistance (Rct) the resistant to the flow of ions and double layer capacitance.
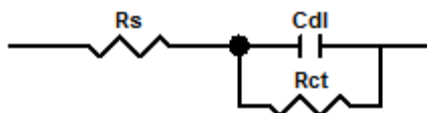

Figure 12. Simplified Randles equivalent circuit for the immunosensor.

Fig.13 shows the Nquist plots for a platinum electrode modified with Co(II)SDD complex, polypyrrole and the corresponding nanocomposite. Lower impedance for Pt/PPy is observed with Rct of 28.8 kΩ in comparison to Rct values of 47.7 kΩ and 54.7 kΩ for Pt/Co(II)SDD and Pt/PPy-Co(II)SDD respectively. Polypyrrole is a thin film conducting polymer in addition to its ionic conductivity [18]. Platinum electrode modified with polypyrrole showed the highest conductivity with respect to the nanocomposite. Cobalt Schiff base complexes has been shown to be electrically conductive and suitable for composite formation with polypyrrole [11].
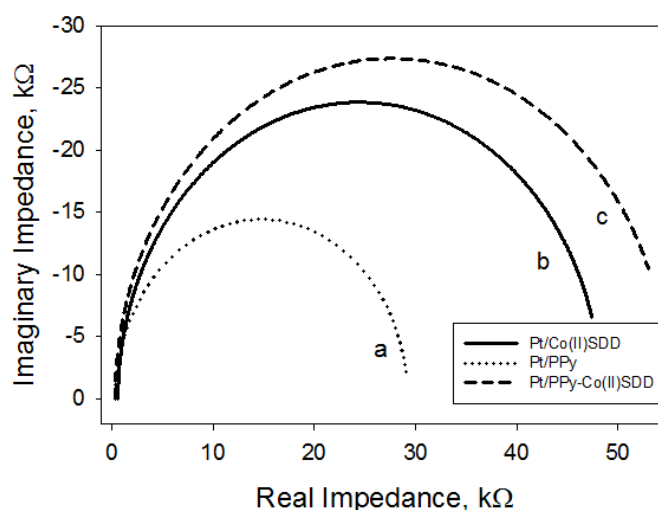

Figure 13. Nquist plot of the, (a) Pt/PPy, (b) Pt/Co(II)SDD and Pt/PPy-Co(II)SDD in 0.1 M phosphate buffer at -600 mV applied potential.

The increase in total impedance of the nanocomposite shows that is less conductive than corresponding pyrrole in Fig.13 (b). This is due to the catalytic behaviour of Co(II)SDD during the

polymerisation process. The increased thickness of polypyrrole when Co(II)SDD is embedded into the polymer, increases the resistance to charge transfer which is due to the decrease in exchange current density (i_o). Electrons are thus travelling to the electrode through further distance than for just Pt/PPy and Pt/Co(II)SDD. The reduced electron transfer rate constant is compensated by an increase in available biocompatible sites for binding to tTG. A decrease in Rct to 31.9 kΩ is observed after immobilization of tTG. The reduced impedance is not commonly observed after immobilization of proteins onto modified electrodes. It can be assumed that the degree of binding allows for charge and electrons to shuttle at the electrolyte/electrode interface with faster heterogeneous rate constant. This direct measurement in phosphate buffer allows the observation for this binding. After blocking of the electrode with BSA, an increase in Rct from 31.9 kΩ to 43.5 kΩ for immunosensor with BSA since there is a slower transfer of electrons and charges across the electrolyte/electrode interface seen in Fig.14.
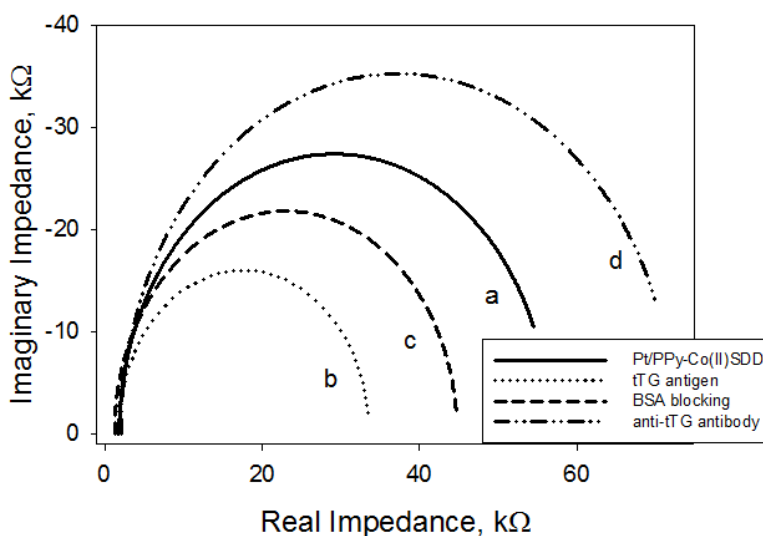

Figure 14. Nyquist plot of, (a) Pt/PPy-Co(II)SDD platform, (b) immunosensor, (c) after BSA blocking of immunosensor and (d) after incubation of anti-tTG antibody in 0.1 phosphate buffer at -600 mV applied potential.

Binding interaction between tTG and anti-tTG at lower concentrations gave lower Rct value for BSA blocking. This is due to binding that allows for electron transfer to occur faster. As concentration of anti-tTG antibody is increased, Rct values increase which indicates more insulating response is observed.

Table 2. Comparison of different immobilization steps.

	Pt/Co(II)SDD	Pt/PPy	Pt/PPy-Co(II)SDD	Pt/PPy-Co(II)SDD/tTG	BSA blocking	Antibody detection
Rs (kΩ)	0.67	0.38	0.58	1.68	1.24	2.05
Cdl (μF)	4.65	3.26	5.78	1.97	1.73	4.38

Rct (kohm)	47.7	28.8	54.7	31.9	43.5	70.4
i_o	5.38×10^{-7}	8.91×10^{-7} 4.5×10^{-7}	8.04×10^{-7}	5.9×10^{-7}	3.64×10^{-7}
k_{et}(cm^2 s^{-1})	2.7×10^{-6}	4.6×10^{-6} 2.33×10^{-6}	4.16×10^{-6}	3.05×10^{-6}	1.88×10^{-6}

Table 2 represents the different parameters used to evaluate different platforms used for the development of the immunosensor for anti-tTG antibody. Important parameters, i_o (exchange current) and k_{et} (heterogeneous rate constant) are calculated from

$$I_o = RT / nFRct,$$

Where R is the gas constant (8.314 J K^{-1} mol^{-1}), F is Faraday constant (96 486 C mol^{-1}), n is the number of electrons, Co is the concentration of the solution (mol cm^{-3}), and

$$k_{et} = i_o / nFAC_o,$$

Where A is area of the electrode (cm^2). The k_{et} was calculated using i_o and was found to be higher for Pt/PPy-Co(II)SDD (2.33×10^{-6} cm^2 s^{-1}) in comparison to a platinum electrode modified with just PPy (4.6×10^{-6} cm^2 s^{-1}) and Co(II)SDD (2.7×10^{-6} cm^2 s^{-1}) suggesting slower electron transfer.

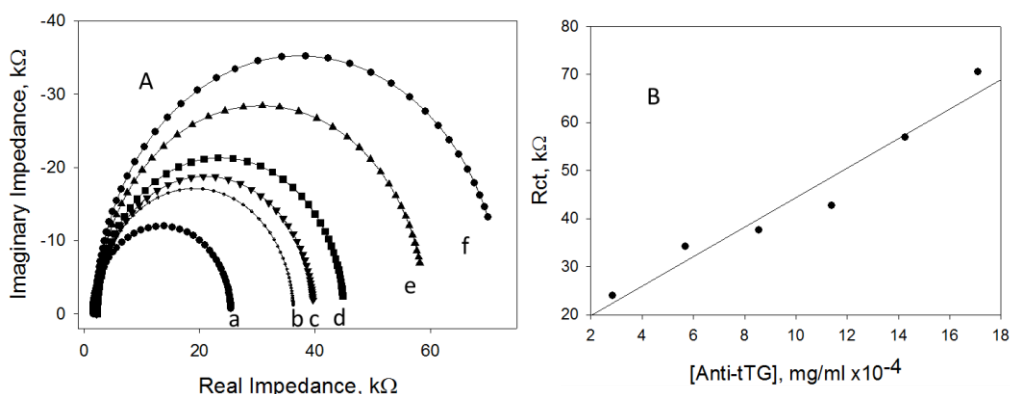**Figure 15.** A) Nyquist plot for anti-tTG antibody incubation at, (a) 2.85×10^{-4} mg mL^{-1}, (b) 5.7×10^{-4} mg mL^{-1}, (c) 8.55×10^{-4} mg mL^{-1}, (d) 11.4×10^{-4} mg mL^{-1}, (e) 14.25×10^{-4} mg mL^{-1}, (f) 17.1×10^{-4} mg mL^{-1} and calibration graph for immunosensor Rct versus anti-tTG antibody concentration in 0.1 M phosphate buffer. B) Calibration plot for the detection of anti-tTG antibody in 0.1 phosphate buffer.

The labeless electrochemical immunosensor was evaluated using different concentrations of anti-tTG antibody produced in goat. The calibration curve for Rct with response values is shown in Fig. 15 B. A linear increase in Rct is observed with increase in concentration of anti-tTG antibody with a linear correlation coefficient of 0.948 in 0.1 M phosphate buffer. A detection limit of 201 ng/mL is estimated with the standard deviation rule.

Table 3 shows the comparison for different strategies for the detection of anti-tTG. Various methods for detection of antigens can be used, each providing different performance parameters. These performance parameters are dependent on the technique used, immobilization strategies, and time of biomolecule immobilization. The different strategies seen table 3, shows how dynamic linear range and limit of detection is altered. Promising new tools such as electrochemical detection strategies

provides rapid detection compared to the conventional enzyme linked immunosorbent assays. This study gave a limit of detection of 201 ng mL^{-1} well below the limit for concentration of transglutaminase in the human body. Compared to table 3, other methods have lower limits of detection with similar linear ranges.

Table 3. Comparison of different detection strategies for anti-tTG antibody.

Method	Dynamic Linear Range	Limit of detection	Reference
Electrochemical (SWV)	$10^{-5} - 10^{-4}$ mg mL^{-1}	52.8 ng mL^{-1}	19
Fluorescence	$10^{-6} - 10^{-5}$ mg mL^{-1}	0.8 ng mL^{-1}	20
Electrochemical (EIS)	$10^{-6} - 10^{-4}$ mg mL^{-1}	5.2 ng mL^{-1}	21
ELISA	-	0.200 ng mL^{-1}	22
Electrochemical (Amperometric)	$1 - 10$ μg mL^{-1}	390 ng mL^{-1}	4

4. CONCLUSION

Polyrrole composites formed with cobalt (II) SDD complex on platinum electrodes showed good recognition and transduction properties for label-free anti-tTG antibody immunosensors. These composites reported here for the first time, allowed the combination of properties of two different materials for increased electrocatalytic efficiency and biocompatibility. Increased biocompatibility allowed for immobilization of biomolecules whilst maintaining their bioactive integrity. Increased available binding sites aided the stabilization of the biomolecule layer. The addition of anti-tTG antibody to the immunosensor resulting in increase in impedance of the sensor, where Rct values were used as evaluating parameter. The EIS data gave a linear correlation as with antigen-antibody concentration dependent binding event. Overall, the performance of this immunosensor enhanced signal response and biomolecule immobilization for selective detection of anti-tTG antibody at concentrations as low as 2.85 x 10^{-4} mg mL^{-1}.

References

1. W. Dieterich, T. Ehnis, M. Bauer, P. Donner, U. Volta, E. Riecken, D. Schuppan. *Nature Medicine*, 3 (1997) 7
2. L. Rivera, J. Sanchez, P. Sanchez, I. Katakis, C. O'Sullivan . *Biosensors and Bioelectronics,* 26 (2011) 4471
3. K. Lindfors, M. Maki, K. Kaukinen. *Autoimmunity Reviews*, 9 (2010) 744
4. S. Dulay, P. Sanchez, E. Iwuoha, I. Katakis, C. O'Sullivan. *Biosensors and Bioelectronics,* 26 (2011) 3852
5. A. Sabatino, A. Vanoli, P. Giuffrida, O. Luinetti, E. Solcia, G. Corazza. *Autoimmunity Reviews,* 11 (2012) 746
6. S. Reif, A.Lerner. *Autoimmunity Reviews,* 3 (2004) 45
7. F. Ricci, G. Adornetto, G. Palleschi. *Electrochimica Acta*, 84 (2012) 74
8. J. Martinovic, A. Paquim, V. Diculescu, J. Van Wyk, E. Iwuoha, P. Baker, S. Mapolie, A. Brett. *Electrochimica* Acta, 53 (2008) 4907
9. S. Niu, F. Li, S. Zhang, L. Wang, X. Li, S. Wang. *Sensors*, 6 (2006) 1234
10. S. Pradeepa, B. Naik, B. Kumar, K. Priyadarsini, A. Barik, T. Naik. *Spectrochimica Acta Part A: Molecular and Biomolecular Spectroscopy*, 101 (2013) 132
11. J. Losada, I. Peso, L. Beyer, J. Hartung, V. Fernandez, M. Mobius. *Journal of Electroanalytical Chemistry*, 398 (1995) 89
12. C. Fuente, J. Acuna, M. Vazquez, M. Tascon, M. Gomez, P. Batanero. *Talanta*, 44 (1997) 685
13. A. Ramanavicius, A. Finkelsteinas, H. Cesiulis, A. Ramanaviciene. *Bioelectrochemistry* 79 (2010) 9
14. A. Ramanavicius, A. Ramanaviciene, A. Malinauskas. *Electrochimica Acta*, 51 (2006) 6025
15. A. Sargent, T. Loi, S. Gal, O. Sadik. *Journal of Electroanalytical Chemistry*, 470 (1999) 144
16. J. van Wyk, S. Mapolie, A. Lennartson, M. Hakansson, S. Jagner. *Inorganica Chimica Acta*, 361 (2008) 2094
17. T. Balkenhohl, F. Lisdat. *Analytica Chimica Acta*, 597 (2007) 50
18. P. Sharma, G. Gupta, V. Singh, B. Tripathi, P. Pandey, M. Boopathi, B. Singh, R. Vijayaraghavan. *Synthetic Metals*, 160 (2010) 2631
19. S. Kergaravat, L. Beltramino, N. Garnero, L. Trotta, M. Wagener, M. Pividori, S. Hernandez. *Biosensors and Bioelectronics*, 48 (2013) 203
20. M. Kergaravat, L. Beltramino, N. Garnero, L. Trotta, M. Wagener, S. Fabiano, M. Pividori, S. Hernandez. *Analytica Chimica Acta*, 798 (2013) 89
21. N. West, P. Baker, T. Waryo, F. Ngece, E. Iwuoha, C. O'Sullivan, I. Katakis. *Journal of Bioactive and Compatible Polymers* 28 (2013) 167
22. J. Wolf, I. Lachmann, U. Wagner, A. Osman, T. Mothes, *Analytical* Biochemistry, 419 (2011) 153